Advances in River Sediment Research – Fukuoka et al. (eds)
© 2013 Taylor & Francis Group, London, ISBN 978-1-138-00062-9

Quasi 3D numerical simulation for flow and bed variation with various sand waves

T. Uchida & S. Fukuoka
Research and Development Initiative, Chuo University, Japan

ABSTRACT: This paper presents a quasi-3D numerical computation method for sand waves varying with hydraulic conditions. To calculate depth scale flow structures interacting with sand waves, we developed the general Bottom Velocity Computation method (general BVC method) based on a depth integrated model, in which bottom velocity and pressure acting on bed surface are calculated semi-directly without taking the assumption of the shallow water flow, such as the hydrostatic pressure distribution. The flow separation behind the dune crest, which has been found to play an important role of the dune formation, is evaluated by the production terms of the depth integrated vorticity equations. Non-equilibrium sediment transport is calculated by using momentum equation of the sediment motion with the lag distance. We applied the model to experimental results on sand waves in a narrow channel and discussed the performance of the model.

1 INTRODUCTION

It is important for understanding dynamics of flow and sediment transport in rivers to evaluate bed resistance with sand waves. The bed resistance is separable into two components. One is the surface resistance due to sediment particles and the other is the form resistance due to sand waves. Generally, compared to the objective flow scale, the sediment particle size is so small that the flow around the particles is simplified as the rough wall low. On the other hand, the scale of the sand wave and surrounding flow would be comparable to the objective scale. Those are in an interacting system. Although many researchers have recognized the need to evaluate dynamics of flow with bed variation in the integrated system of sediment transport, sand waves and bed resistance (e.g., Kennedy, 1963; Ashida & Michiue, 1972; Task Committee of JSCE, 1973; Fukuoka et al., 1982), most of previous bed variation analyses have assumed the sand waves as the bed resistance for simplification (e.g., Fukuoka, 2005; Wu, 2008). It is considered for the reason that 2D model without the ability to calculate vertical distributions of velocity and pressure intensity cannot evaluate the interactions among sand waves, sediment transport and bed resistance. There are a lot of studies on turbulence and vortex motions in the vicinity of sand dunes (e.g., Best, 2005). Recently, some researchers succeeded in simulating dune formations in a narrow channel by vertical two-dimensional turbulence model (Giri & Shimizu, 2006; Niemann et al., 2011). For analogous phenomena of the bed variation with sand waves, local scouring just downstream from a groundsill in a laboratory channel could be reproduced by the vertical 2D model (Uchida et al., 2004). However, it would be unrealistic to apply these models to 3D flows and bed morphology in rivers because of extremely high computational cost.

It has been commonly known that the type of bed forms can be classified by 1D parameters such as Froude number. The fact would implicate that the sand wave structures developed to the depth scale are controlled by the depth scale dynamics of flows. For the calculations of flood flows and bed variations in rivers, the turbulence 3D model with the resolution capability of turbulent motions near the bed is not always indispensable, because the effects of sand waves on large scale phenomena of sediment transport and flow resistance are important to be evaluated rather than the small scale phenomena of the turbulence motions. However, few researchers have focused on the method for the above purpose. Onda & Hosoda (2004) proposed the depth integrated model based on one dimensional Boussinesq equation to compute processes of sand waves developing and decaying due to changing in the channel slope. They added the effects of acceleration-deceleration near the bottom to the irrotational flow conditions for evaluating bed shear stress on sand waves. In their method, it would be difficult to evaluate vorticity supply due to the flow separation behind the dune crest, which has been found to play an important

role of the dune formation. For the condition of a steep channel, the flow separations at hydraulic jumps should also be taken into account.

Uchida & Fukuoka (2012a, b) have developed a new depth integrated model for reasonable bed variation analysis, the general Bottom Velocity Computation (BVC) method, to evaluate velocity and pressure acting on bed surface semi-directly without calculating those vertical distributions and assuming the shallow water flow. They have applied the method to 3D local flow structures with horseshoe vortex around a cylinder (Uchida & Fukuoka, 2012a) and rapidly varied flows over structures (Uchida & Fukuoka, 2012b). The objective of this study is to develop the general BVC method with a sediment transport model for sand waves varying with hydraulic conditions.

2 CALCULATION METHOD

2.1 *Frame work of the BVC method without assumptions of the shallow water flow*

It is important for bed variation analyses with sand waves to appropriately evaluate the longitudinal distribution of sediment transport rate affected by bed forms (Kennedy, 1963). The general BVC method presented in this paper (Fig. 1) makes possible to calculate bottom velocity distribution controlling sediment motions without the assumption

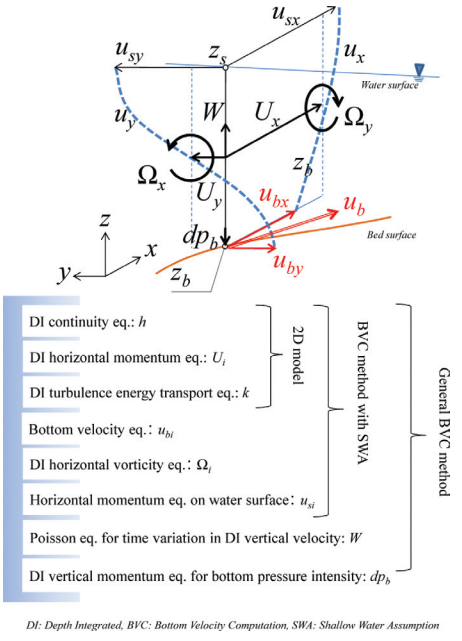

Figure 1. Framework of the BVC method.

of the shallow water flow such as hydrostatic pressure distribution. The bottom velocity varies with bed shear stress acting on bed surface and pressure distribution by the bed forms. The former effects are evaluated in the present model mainly by the changes in depth averaged velocity due to bed shear stress and vertical velocity distribution due to vorticity supply from the bed surface. To consider the latter effects, the spatial variation term in vertical velocity in Equation (1) and non-hydrostatic pressure terms in Equation (5) and (11) are important. And the bottom pressure intensity is necessary to evaluate the resistance of the sand waves. Those terms have been neglected in many previous depth integrated models with the shallow water assumption. The general BVC method without assuming the shallow water flows (Uchida & Fukuoka, 2012a) is necessary to calculate bed variation with sand waves.

The important equation of the BVC method is the bottom velocity equations (1), which is derived by depth-integrating horizontal vorticity.

$$u_{bi} = u_{si} - \varepsilon_{ij3}\Omega_j h - \frac{\partial Wh}{\partial x_i} + w_s \frac{\partial z_s}{\partial x_i} - w_b \frac{\partial z_b}{\partial x_i} \qquad (1)$$

where, i, j = 1(x), 2(y), e_{ij3}: Levi-Civita symbol, u_{bi}: bottom velocity, u_{si}: water surface velocity, Ω_j: Depth Averaged (DA) horizontal vorticity, h: water depth, W: DA vertical velocity, z_s: water level, z_b: bed level, w_s, w_b: vertical velocity on water surface and bottom, respectively. The bottom pressure intensity is also important and given by Eq. (2) integrated the vertical momentum equation with respect to the vertical direction for water depth, neglecting unsteady and horizontal shear stress terms.

$$\frac{dp_b}{\rho} = \frac{\partial hWU_j}{\partial x_j} + \frac{\tau_{bj}}{\rho}\frac{\partial z_b}{\partial x_j} \qquad (2)$$

where, dp: pressure deviation from hydrostatic pressure distribution ($p = \rho g\,(z_s - z) + dp$), dp_b: dp on bottom, U_j: DA horizontal velocity, τ_{bj}: bed shear stress. By using Eq. (1) and Eq. (2), the BVC method allows semi-direct computations of bottom velocity and bottom pressure intensity without computing those vertical distributions.

2.2 *Governing equations of the BVC method*

To evaluate bottom velocity and bottom pressure intensity by Eqs. (1) and (2), the BVC method solves equations for the following unknown quantities: water depth h, DA horizontal velocity U_i, DA turbulence kinetic energy k, DA horizontal vorticity Ω_i, horizontal velocity on water surface u_{si},

DA vertical velocity W. These equations are derived by using cubic vertical velocity distribution:

$$u_i = U_i + \Delta u_i\left(12\eta^3 - 12\eta^2 + 1\right) - \delta u_i\left(4\eta^3 - 3\eta^2\right) \quad (3)$$

where, $\Delta u_i = u_{si} - U_i$, $\delta u_i = u_{si} - u_{bi}$, $\eta = (z_s - z)/h$. And the linear distribution of dp is assumed ($dp = \eta/dp_b$).

Water depth h and DA horizontal velocity U_i are solved by Depth Integrated (DI) continuity equation (4) and DI horizontal momentum equations (5):

$$\frac{\partial h}{\partial t} + \frac{\partial U_j h}{\partial x_j} = 0 \quad (4)$$

$$\frac{\partial U_i h}{\partial t} + \frac{\partial U_i U_j h}{\partial x_j} = -gh\frac{\partial z_s}{\partial x_i} - \frac{\tau_{bi}}{\rho} + \frac{\partial h\tau_{ij}}{\rho\partial x_j} - \left(\frac{\partial h dp_0}{\rho\partial x_i} + \frac{dp_b}{\rho}\frac{\partial z_b}{\partial x_i}\right) \quad (5)$$

where, $\tau_{ij} = \nu S_{ij} + \overline{u_i' u_j'}$, $\nu = \nu_m + \nu_t$, ν_m: kinematic viscosity coefficient, ν_t: kinematic eddy viscosity coefficient, S_{ij}: DA strain velocity, $u_i' = u_i - U_i$. In this paper, superscript bar indicates depth integrated value and evaluated by vertical velocity distribution (3).

For the kinematic eddy viscosity coefficient, this study employs one equation model:

$$\frac{\partial k}{\partial t} + U_j\frac{\partial k}{\partial x_j} = \frac{1}{h}\frac{\partial}{\partial x_i}\left(\frac{\nu h}{\sigma_k}\frac{\partial k}{\partial x_i}\right) + P_k - \varepsilon \quad (6)$$

where,

$$\frac{P_k}{\nu_t} = 2\left(S_{ij}^2 + \overline{s'^2_{ij}}\right) + C_h\left(\frac{\delta u_i}{h}\right)^2, \quad \nu_t = C_\mu\frac{k^{1/2}}{\varepsilon},$$

$C_\mu = 0.09$, $\varepsilon = C_\varepsilon k^{3/2}/\Delta$, $C_\varepsilon/\Delta = 1.7/h$, $C_h = 9(\alpha C_\varepsilon)^4/C_\mu^3$, $\alpha = \kappa/6$, $\kappa = 0.41$, s'_{ij}: strain velocity of deviation velocity u_i'. The Eq. (4) is calculated with $U_i h$ at $n + 1$ step by the following equation for time variation of water depth:

$$\frac{\partial}{\partial x_j}\left((C\Delta t)^2\frac{\partial\phi}{\partial x_j}\right) + \phi^P - \phi = 0 \quad (7)$$

where, Δt: time interval of the numerical integration, f^n, f^{n+1}: a value of f at the n, $n + 1$ time step in the numerical calculation, respectively, f^p: predicted value of f for the $n + 1$ step including n step's variable, $\phi = h^{n+1} - h^n$, $\phi^P = h^P - h^n$, $C^2 = gh$, h^P: predicted water depth by Eq. (4) with $(u_i h)^P$, $(u_i h)^P$: predicted horizontal flux by Eq. (5) with $h = h^n$.

The equations for horizontal voticity are described:

$$\frac{\partial\Omega_i h}{\partial t} = ER_{\sigma i} + P_{\omega i} + \frac{\partial h D_{\omega ij}}{\partial x_j} \quad (8)$$

where, $ER_{\sigma i}$: rotation term of vertical vorticity ($ER_{\sigma i} = u_{si}\omega_{\sigma s} - u_{bi}\omega_{\sigma b}$), $\omega_{\sigma s}$, $\omega_{\sigma b}$: rotation of u_{si}, u_{bi}, respectively, $P_{\omega i}$: production term of vorticity from the thin bottom vortex layer, $D_{\omega ij}$: horizontal vorticity flux due to convection, rotation, dispersion and turbulence diffusion. The production terms and horizontal vorticity flux are:

$$P_{\omega i} = C_{p\omega}\nu_{tb}\frac{\omega_{bei} - \omega_{bi}}{h} \quad (9)$$

$$D_{\omega ij} = \overline{\omega_j u_i} - \overline{\omega_i u_j} + \frac{\nu_t}{\sigma_\omega}\frac{\partial\Omega_i}{\partial x_j} \quad (10)$$

where, $C_{p\omega} = \kappa/\alpha$, ν_{tb}: ν_t on the bottom converted into depth averaged scale, ω_{bi}: horizontal vorticity on bottom, ω_{bei}: equilibrium ω_{bi} for u_{bi} (Eq. 18), $\sigma_\omega = 1$. ω_i is evaluated by the vertical differentiation of Eq. (3).

The equations for water surface velocity are derived by assuming very thin layer under the water depth ($\delta z_s \to 0$, δz_s: thickness of the water surface layer):

$$\frac{\partial u_{si}}{\partial t} + u_{sj}\frac{\partial u_{si}}{\partial x_j} = -\left\{g + \left(\frac{\partial dp}{\partial z}\right)_{z=z_s}\right\}\frac{\partial z_s}{\partial x_i} + P_{si} \quad (11)$$

where, P_{si} is shear stress under the water surface layer and evaluated by using Eq. (3):

$$P_{si} = \frac{2\nu_t}{h^2}\left\{12\left(u_{sei} - u_{si}\right) - \left(3\delta u_i - 6\Delta u_i\right)\right\} \quad (12)$$

where, u_{sei}: equilibrium water surface velocity $u_{sei} = U_i + (\delta u_i - \Delta u_i)/2$.

The time variation in the DI vertical velocity calculated by Eq. (7) with $\phi = (Wh)^{n+1} - (Wh)^n$, $\phi^P = (Wh)^P$, $C = k_1 h/\Delta t$, $k_1 = 1/20$. $(Wh)^P$ is calculated by the continuity equation with horizontal velocity field by using predicted bottom velocity $(u_{bi})^P$:

$$(Wh)^P = \frac{\partial}{\partial x_j}\left[(h^2)^{n+1}\left\{k_2(\Delta u_j)^{n+1} - k_1(\delta u_j)^P\right\}\right] + h^{n+1}\left(\frac{\partial z_m}{\partial t} + U_j\frac{\partial z_m}{\partial x_j}\right)^{n+1} \quad (13)$$

where, $k_2 = 1/10$, $(\Delta u_i)^P = (u_{si})^{n+1} - (u_{bi})^P$, $(u_{bi})^P$ is evaluated by Eq. (1) with $(Wh)^n$, $z_m = (z_s + z_b)/2$.

2.3 *Evaluation method for flow separation behind the crest on dune and hydraulic jump*

The flows with sand waves are characterized by flow separation behind the dune crest and wave breaking at the hydraulic jump (e.g., Kennedy, 1963; Task Committee of JSCE, 1973; Fukuoka et al., 1982). It is important for flow and bed variation analysis with sand waves to evaluate these flow separations at bed and water surfaces. The present analysis uses the criterion variation in bed and water surface gradients for the flow separation. The values of 1/10 and 1/5 are setting for flow separations criterions for bed and water surface, respectively, referring to previous study (Uchida, 2011; Uchida 2012b). To consider vorticity production due to bottom flow separation and breaking wave, following vorticity fluxes are added in the production terms:

(Bottom flow separation)

$$P_{\omega sbi}\Delta x = \begin{cases} -\varepsilon_{ij3}\left|u_{bj'}/2\right|\cdot u_{bj} & (+\varepsilon_{ij3}\delta z_{bj} > 1/10) \\ 0 & (+\varepsilon_{ij3}\delta z_{bi} < 1/10) \end{cases} \quad (14)$$

(Breaking wave)

$$P_{\omega ssi}\Delta x = \begin{cases} +\varepsilon_{ij3}\left|u_{sj'}/2\right|\cdot u_{sj} & (-\varepsilon_{ij3}\delta z_{sj} > 1/5) \\ 0 & (-\varepsilon_{ij3}\delta z_{sj} < 1/5) \end{cases} \quad (15)$$

where, $j' = j$, δz_{bj}, δz_{sj}: variations in bed, water surface gradients between the two neighbor grids in j direction, respectively. For the breaking wave, following conditions are added. One is the discontinuity condition for the advection terms in the water surface velocity equation. The surface velocity at the breaking point is set to zero for the advection term. The other is the pressure intensity just downstream of the breaking wave point is set to zero, if negative pressure intensity is calculated by Eq. (2).

2.4 *Evaluation method of bed shear stress and bed tractive force*

The wall low at roughness bed is important to evaluate bed tractive force for sediment transport rate. The definition of the relationship between the bottom height for bed shear stress and the height of the surface sediment particle should be made for this purpose (e.g., Colombini, 2004). The logarithmic velocity distribution law cannot be applied under the particle surfaces, because of their drag forces. The bottom height in this paper is defined as Figure 2.

The bottom level z_b to evaluate bed shear stress is defined as $z_b = \delta z_b + z_g$ (z_g: top height of the surface particle, δz_b: very thin vortex layer).

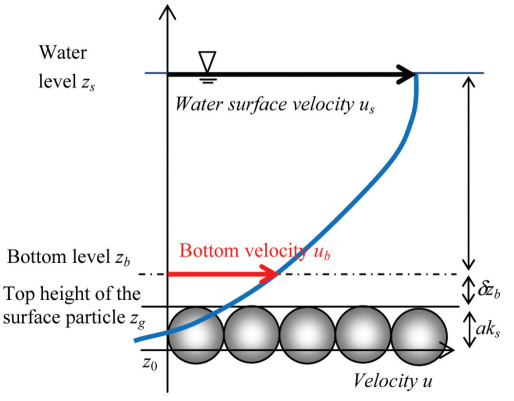

Figure 2. Definitions of heights of bottom and sediment particles.

The origin of the logarithmic law z_0 is found to be defined as the volume averaged height of the surface particle (Colombini, 2004). However, it is known that the origin level depends on the sediment particle conditions (e.g., Uchida et al., 2001). In this paper, the origin level z_0 is defined by the top height of the surface particle z_g, equivalent roughness k_s and coefficient a ($z_0 = z_g - ak_s$). And this paper sets $a = 1$ for simplicity. The thickness of the vortex layer on the bed is defined as $h/\delta z_b = e^3 - 1$ to satisfy the vertical velocity distribution for uniform flow:

$$u_i = \frac{\delta u_i}{3}\left(1 - 3\eta^2\right) + U_i \quad (16)$$

Assuming very thin thickness of the vortex layer, we can evaluate bed shear stress τ_b and equilibrium vorticity ω_{be} on the bottom:

$$\frac{\tau_b}{\rho} = u_*^2 = (c_b u_b)^2, \quad \frac{1}{c_b} = 8.5 + \frac{1}{\kappa}\ln\left(\frac{\delta z_b + ak_s}{k_s}\right) \quad (17)$$

$$\omega_{be} = 2\frac{u_*}{\kappa h}\ln\left(\frac{\delta z_b + ak_s + h}{\delta z_b + ak_s}\right) \quad (18)$$

The bed surface disturbance growing into sand waves would be created mainly by unsteady 3D turbulence motions in the vicinity of the bed. The additional term of the disturbance is needed for the present method based on the depth integrated model. Although many methods for adding the disturbance are considered, a simple way should be required for the application to flood simulations in rivers. This paper gives the fluctuation of bed tractive force due to turbulence motions whose scale is smaller than the water depth.

$$\tau_* = (1+\alpha_B)\frac{u_*^2}{\sigma g d}$$
$$\alpha_B = A_B \cos\left\{2\pi\left(\frac{x+y}{L}+\frac{t}{T}\right)\right\} \quad (19)$$

where, L and T: spatial and temporal scales of the disturbance, respectively. Although the fluctuation α_B is affected by local turbulence conditions, this paper gives $L = h$, $T = L/u_b$, $A_B = 1.0$, for simplicity. We confirmed that the effects of these parameter in the Eq. (19) on the developed form of sand waves can be negligible.

2.5 *Governing equation for non-equilibrium sediment transport rate with sand waves*

It is important for bed variation analysis with sand dunes to evaluate non-equilibrium sediment motion over them (Giri & Shimizu, 2006; Niemann et al., 2011). In this study, the non-equilibrium sediment motion is calculated by the sediment particle momentum equation (Uchida & Fukuoka, 2011):

$$\frac{\partial q_{Bi}}{\partial t}+\frac{\partial u_{Bj}q_{Bi}}{\partial x_j} = \left(Pu_{BPi}-Du_{BDi}\right)+m_* h_B\left(\gamma_{ei}-\gamma_i\right) \quad (20)$$

where, q_{Bi}: bed load sediment transport rate vector, u_{Bi}: particle velocity vector of bed load, Pu_{BPi}: particle momentum from bed material, Du_{BDi}: loss of particle momentum due to particles deposition, $m_* = \mu_k\, sg\cos\theta/(s+1+C_M)$, C_M: coefficient of added mass, μ_k: dynamic friction coefficient of particles, s: specific gravity of sediment in water, θ: bed gradient, h_B: apparent thickness of bed load ($h_B = q_B/u_B$), $q_B^2 = q_{Bi}q_{Bi}$, $u_B^2 = u_{Bi}u_{Bi}$, γ_i, γ_{ei}: unit vector of sediment movement and that for the equilibrium condition, respectively. This paper gives the first term in Eq. (20) and the apparent thickness h_B and velocity u_B of bed load as (Uchida & Fukuoka, 2011):

$$Pu_{BPi}-Du_{BDi} = q_{Be}u_{Bei}/L_e - q_B u_{Bi}/L \quad (21)$$

$$\begin{cases} u_B/\sqrt{sgd} = 3.3\left(q_{B*}\right)^{1/3},\ u_{Be}/\sqrt{sgd} = 3.3\left(q_{Be*}\right)^{1/3} \\ h_B/d = 0.3\left(q_{B*}\right)^{2/3} \end{cases} \quad (22)$$

where, L: lag distance of bed load motion, L_e, q_{Be}, u_{Bei}: equilibrium lag distance, sediment transport rate and apparent velocity of bed load corresponding to local bed tractive force, respectively, $u_{Be}^2 = u_{Bei}u_{Bei}$, $q_{B*} = q_B/(sgd^3)^{1/2}$, $q_{Be*} = q_{Be}/(sgd^3)^{1/2}$.

The equilibrium sediment transport rate is calculated by the Ashida & Michiue Formura (1974). The lag distance is important parameter to determine non-equilibrium sediment motion, correlating sediment transport rate with deposition and pick-up rates. Although some empirical formulae for the lag distance have been proposed (e.g., Phillips & Sutherland, 1989; Fukuoka, 2005; Wu, 2008), those applicability to sand waves calculation has not been clarified. The lag distance is identified as the average particle step length for uniform flow condition without varying in bed tractive force. However, for the non-equilibrium flow condition with sand waves, the lag distance would be decreased due to acceleration and deceleration of bottom velocity. At present, its evaluation method has not been established yet. This paper uses equation (23) for the lag distance, which is transformed from the previous empirical equations to apply bed variation analysis (Uchida & Fukuoka, 2011), adjusting coefficient α_L to reproduce experimental results by the calculation.

$$L_e/d = \alpha_L\left(q_{Be*}\right)^{2/3},\ L/d = \alpha_L \max\left(q_{Be*}, q_{B*}\right)^{2/3} \quad (23)$$

As increasing α_L in Eq. (23), the wave length is increasing with decreasing in the wave height, and the plane bed appears eventually. This study sets $\alpha_L = 7$, considering that the lag distance is shorter than the average particle step length.

The temporal variation in the bed elevation is computed with neglecting variations in apparent thickness of bed load:

$$(1-\lambda_B)\frac{\partial z_B}{\partial t}+\frac{\partial q_{Bi}}{\partial x_i} = 0 \quad (24)$$

where, λ_B: the porosity of bed material ($\lambda_B = 0.4$).

3 CALCULATION RESULTS AND DISCUSSIONS

3.1 *Calculation conditions*

This study applies the present method to experiments on the sand waves conducted in the narrow channel by Fukuoka et al. (1982). This experiment investigated flow and sediment transport rate with various types of sand waves generated in the acrylic channel with 0.04 m width and 8.0 m long for diverse hydraulic conditions of bed slope, sediment particle diameter and water discharge. Refer to the literature (Fukuoka et al., 1982) for details of the experimental conditions and results. This paper presents calculation results on a part of their experimental cases, as shown in Table 1. The boundary conditions of the upstream end for calculations are given by the experimental discharge. The shear stress acting on bed and side wall are

Table 1. Hydraulic conditions for various bed forms experiment (Fukuoka et al., 1982).

Case	I	q (m²/s)	d (mm)	Fr	Sand wave type	
					Experiment	Calculation
1	1/178	43.0×10^{-3}	0.76×10^{-3}	0.66	Dune	Dune
2	1/147	43.0×10^{-3}	0.76×10^{-3}	0.65	Duen	Dune
3	1/73.0	44.3×10^{-3}	0.76×10^{-3}	0.88	Anti-dune moving downstream	Dune with long wave length
4	1/31.0	39.5×10^{-3}	0.76×10^{-3}	1.74	Plane bed	Plane bed
5	1/31.0	10.8×10^{-3}	0.19×10^{-3}	1.11	Anti-dune	Anti-dune
6	1/31.0	26.8×10^{-3}	0.19×10^{-3}	1.24	Anti-dune	Anti-dune
7	1/20.0	13.3×10^{-3}	0.19×10^{-3}	0.65	Anti-dune	Anti-dune

I: channel slope, q: discharge per unit width, d: sediment particle diameter, Fr : averaged Froude number, $\mathrm{Fr} = q/(\mathrm{gh}^3)^{0.5}$ (Local Fr varies longitudinally especially for case 5~7).

evaluated with equivalent roughness $k_s = d$ (d: sediment particle diameter) and Manning's roughness coefficient $n = 0.008$, respectively. The computational mesh size is set to $dx = dy = 0.01$ m to calculate the depth scale vortex motion. For the initial condition, flow calculation results with flat fixed bed are given. Table 1 shows sand wave types in the measurements and calculations. Although the regime of anti-dune moving downstream for Case 3 was not appear in the present calculation, the three different types of dune, plane bed and anti-dune were reproduced by the general BVC method with non-equilibrium sediment transport model. The followings are discussions on calculation results for each sand wave type.

3.2 *Dunes (Case 1, Case 2)*

Figure 3 shows the developing stage of dune formation for Case 2. The Froude Number for the initial condition is larger than Fr = 0.8. We can see that water depth increases with developing the bed form disturbance. At the initial stage (0.5 min), the bed form disturbance grows up locally, and then small dunes with short wave length appear in the whole of the channel (1.0 min). These dunes grow up with dune coalescences moving downstream and become dunes with long wave length (2.0 min). After that, the average size of sand dunes and water depth do not change (4.0 min). However, dune sizes are different from each other and a dune moves downstream with dune coalescences and breakups.

Followings are discussions on the results for developed dunes. Figure 4 shows computed velocity distributions of flows with developed dunes for Case 2. We can see relatively high velocity at the middle depth and low velocity at the water surface on the dune crest. These velocity distributions are generated under the non-hydrostatic pressure distributions by the effects of the dune shape. The calculation results describe characteristics of bottom velocity of flows with sand dunes: low bottom velocity in the separation zone behind the dune crest, accelerating downstream of the

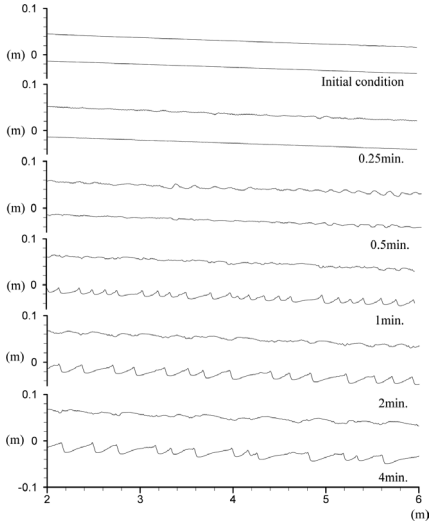

Figure 3. Developing stage of dune formation for Case 2.

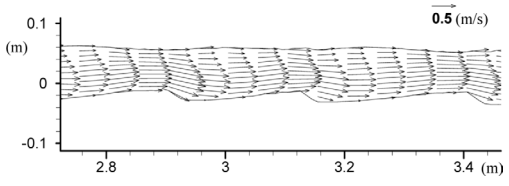

Figure 4. Computed velocity distributions with developed dunes for Case 2.

reattachment point of the separation, and high bottom velocity on the crest. The computed dune has a mild slope with upward convex upstream of the crest and a sharp slope downstream of it, whose characteristics have been investigated in the previous study (e.g., Kennedy, 1963). Figure 5 shows computed water surface and bed profiles for Case 1 and Case 2. Table 2 shows quantitative comparisons between measured and computed results of averaged water depth, sediment discharge per unit width, wave length, wave celerity, and wave height of dunes. It is noticed that computed water depth are larger than measured depths and computed wave lengths are longer than measured wave lengths. Although computed wave celerity is lower than measured one, averaged wave heights $k_d = 2q_B/C$ using calculation results are larger than those of measurements. These results indicate that sand dunes in the calculation are more developed compared with those in the experiment, calculating large dune resistance. However, resulting differences of water depth and sediment discharge between measured and calculated results are not so large. Therefore it would be safe to say that the present calculation method can reproduce the qualitative and quantitative characteristics of sand dunes generated in the experiments.

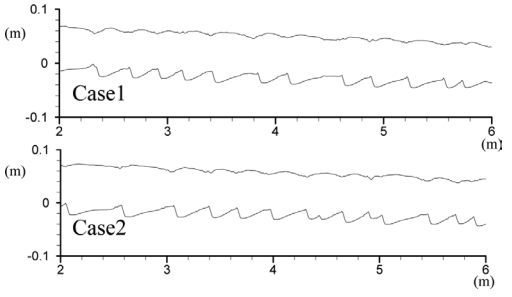

Figure 5. Computed water surface and bed profiles for Case 1 and Case 2.

Table 2. Measured and computed data for Case 1 and Case 2.

	h (m)	q_B (m²/s)	L (m)	C (m/s)	k_d (m)
Case 1					
Exp.	0.074	1.8×10^{-5}	0.17	5.7×10^{-3}	6.3×10^{-3}
Cal.	0.079	1.4×10^{-5}	0.26	2.4×10^{-3}	11.6×10^{-3}
Case 2					
Exp.	0.077	2.0×10^{-5}	0.25	7.8×10^{-3}	5.1×10^{-3}
Cal.	0.079	1.8×10^{-5}	0.30	3.0×10^{-3}	12.0×10^{-3}

h: averaged water depth, q_B: averaged sediment discharge per unit width, L: averaged wave length of sand dunes, C: averaged wave celerity of sand dunes, k_d: average wave height of sand dunes ($k_d = 2q_B/C$).

3.3 *Plane bed and anti-dune moving downstream (Case 3, Case 4)*

Figure 6 shows computed water surface and bed profiles for Case 3 and Case 4. Table 3 shows quantitative comparisons between measured and computed results of sand waves. In the experiment, anti-dunes moving downstream were observed for the condition of Case 3. This kind of sand waves also occurred in the other experimental conditions (Fukuoka et al., 1982). However, flat dunes with long wave lengths are computed for the Case 3. The computed wave length and wave celerity are much larger than those of measured results. On the other hand, differences between measured and computed water depth and sediment discharge seem to be small. This result would indicate that the resistance of the anti-dunes moving downstream is smaller than that of the dunes. More detailed discussions on the anti-dune moving downstream are future tasks. For the condition of Case 4, plane beds appear both in the experiment and computation.

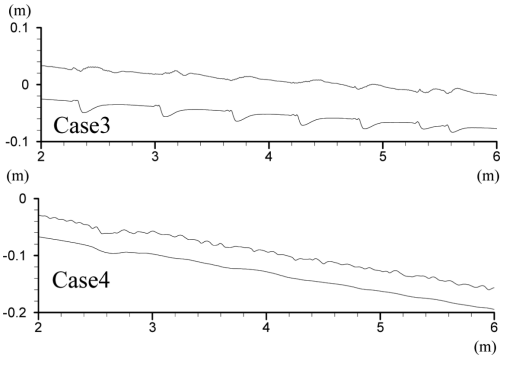

Figure 6. Computed water surface and bed profiles for Case 3 and Case 4.

Table 3. Measured and computed data for Case 3 and Case 4.

	h (m)	q_B (m²/s)	L (m)	C (m/s)
Case 3				
Exp.	0.064	4.7×10^{-5}	0.23	7.6×10^{-3}
Cal.	0.063	8.9×10^{-5}	0.48	1.7×10^{-3}
Case 4				
Exp.	0.037	2.3×10^{-4}	Plane bed	
Cal.	0.037	4.9×10^{-4}	Plane bed	

The computed water depth is almost the same as the measured depth. And the rapidly increased sediment discharge in the experimental result of Case 4 compared with Case 1~3 is well-explained by the calculation.

3.4 *Anti-dunes (Case 5~7)*

Figure 7 shows longitudinal water surface profiles and bed topographies for Case 5~7. Table 3 shows data of sand waves in the experiment and the calculation for Case 5~7. In the present calculation, anti-dunes moving upstream are generated as the experimental results. For the condition, generations and disappearances of anti-dunes and hydraulic jumps are seen successively (Fig. 7 shows snap shots when hydraulic jumps appear). Therefore, temporal changes in the hydraulic conditions for Case 5~7 are large. Table 4 presents the maximum amplitudes with average values. The computed water depths are smaller than those of measured results. One of the reasons would be large temporal and spatial variations in water depth. We can see large temporal variations in sediment discharge, especially 70% fluctuations for Case 7. The averaged sediment discharges in the experiment are almost reproduced by the calculation. The computation results could explain the wave lengths and wave celerity for anti-dune conditions.

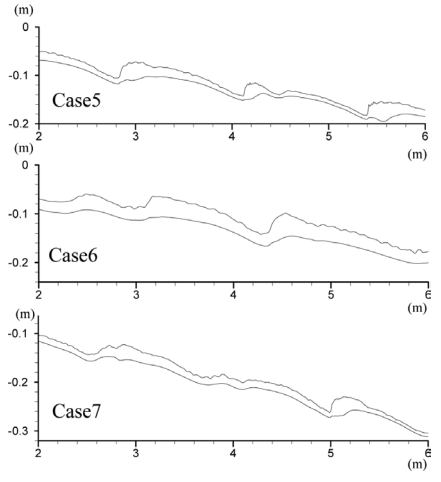

Figure 7. Computed water surface and bed profiles for Case 5~7.

Table 4. Measured and computed data for Case 5~7.

	h^* (m)	q_B^* (m^2/s)	L^* (m)	C (m/s)
Case 5				
Exp.	0.021	1.1×10^{-4}	0.57	-8.1×10^{-3}
Cal.	0.016 ± 0.003	$(1.9 \pm 0.6) \times 10^{-4}$	1.2 ± 0.1	-1.3×10^{-2}
Case 6				
Exp.	0.036	2.7×10^{-4}	1.5	-1.2×10^{-2}
Cal.	0.030 ± 0.002	$(2.8 \pm 0.6) \times 10^{-4}$	1.5 ± 0.2	-1.6×10^{-2}
Case 7				
Exp.	0.035	3.2×10^{-4}	0.78	-9.2×10^{-3}
Cal.	0.016 ± 0.005	$(2.9 \pm 1.8) \times 10^{-4}$	1.2 ± 0.4	-2.0×10^{-2}

*: Computed values indicate averaged value ± maximum amplitudes for channel center (x = 3~6 m).

4 CONCLUSIONS

This study developed the general BVC method with non-equilibrium sediment transport model to calculate bed variation with sand waves for various hydraulic conditions. The present method was able to calculate three different types of sand waves: dune, plane bed and anti-dune and to describe the magnitude of sand waves, water depth and sediment transport rate in the experiment. The governing equations in the present method were derived from Reynolds-averaged Navier-Stokes equations without the shallow water assumption, using vertical velocity and pressure distributions. Non-equilibrium sediment motion was calculated by sediment particle momentum equations. We did not employ special formulae and coefficients, except for bed tractive force fluctuations (Eq. 19) and the lag distance (Eq. 23). Because little influence of parameter variations in Eq. (19) on developed sand wave conditions are confirmed, it would be emphasized that the present method could explain characteristics of various kinds of sand waves with constant parameter of Eq. (23). We plan to develop the method to calculate flood flows and bed variations in river with 3D sand waves.

REFERENCES

Ashida, K. and Michiue, M. 1972. Study on hydraulic resistance and bed-load transport rate in alluvial streams, *Proc. of JSCE* 206:59–69.

Best, J. 2005. The fluid dynamics of river dunes: A review and some future research directions, *J. Geophys. Res.* 110 F04S02, doi:10.1029/2004JF000218.

Colombini, M. 2004. Revisiting the linear theory of sand dune formation, *J. Fluid Mech.* 502:1–16.

Fukuoka, S. 2005. Flood Hydraulics and River Channel Design, Morikita publishing company.

Fukuoka, S., Okutsu, K. and Yamasaka, M. 1982. Dynamic and kinematic features of sand waves in upper regime, *Proc. of JSCE* 323:77–89.

Giri, S. and Shimizu, Y. 2006. Numerical computation of sand dune migration with free surface flow, *Water Resources Researches*, Vol. 42, W10422, doi:10.1029/2005WR004588.

Kennedy, J.F. 1963. The mechanics of dunes and antidunes in erodible-bed channel, *J. Fluid Mech.* 16:521–544.

Niemann, S.L., Fredsøe, J. and Jacobsen, N.G. 2011. Sand dunes in steady flow at low Froude numbers: dune height evaluation and flow resistance, *J. Hydraul. Eng.* 137(1):5–14.

Onda, S. and Hosoda, T. 2004. Numerical simulation on development process of dunes and flow resistance, *Annual Journal of Hydraulic Engineering JSCE* 48:973–978.

Phillips, B.C. and Sutherland, A.J. 1989. Spatial lag effects in bed load sediment transport, *J. Hydraul. Res.* 27(1):115–133.

Task Committee on the Bed Configration and Hydraulic Resistance of Alluvial Streams, Committee on Hydraulic and Hydraulic Engineering, JSCE. 1973. The Bed configuration and roughness of alluvial streams, *Proc. of JSCE* 210:65–91.

Uchida, T. and Fukuoka, S. 2011. A bottom velocity computation method for estimating bed variation in a channel with submerged groins, *Journal of JSCE Ser. B1 (Hydraulic Engineering)* 67(1):16–29.

Uchida, T. and Fukuoka, S. 2012a. Bottom velocity computation method by depth integrated model without shallow water assumption, *Journal of JSCE Ser.B1 (Hydraulic Engineering)* 68(4):I_1225-I_1230.

Uchida, T. and Fukuoka, S. 2012b A computation method for flow over structures, *Advances in River Engineering* 18:351–356.

Uchida, T., Fukuoka, S., Fukushima, T. and Tanaka, M. 2001. Two-dimensional shallow water analysis over large roughness elements and its application, *Journal of Hydraulic Coast and Environmental Engineering JSCE* 691/II-57:93–104.

Uchida, T., Fukuoka, S. and Watanabe, A. 2004. Vertical two-dimentional analysis for local scour just downstream from a groundsill, *Journal of Hydraulic Coast and Environmental Engineering JSCE* 768/II-68: 45–54.

Wu, W. 2008. Computational river dynamics, Taylor & Francis, London.